Experimental considerations in superconductor gravity experiments

Article · January 2012

DOI: 10.2174/978160805399511201010203

CITATIONS
5

READS
197

2 authors, including:

George D Hathaway
Hathaway Research International Inc
14 PUBLICATIONS **80** CITATIONS

SEE PROFILE

CHAPTER 10

Experimental Considerations in Superconductor Gravity Experiments

George Hathaway[1,*] and Harald Reiss[2]

[1]Hathaway Consulting Services, 1080 19th Sideroad, King City, Ontario, Canada L7B 1K5 and [2]Department of Physics, University of Wuerzburg, Am Hubland, D-97074 Wuerzburg, Germany

Abstract: Reports of experimental modifications of gravity over rotating superconductors or of a weight increase or decrease during cool-down of superconductors have prompted many researchers to consider designing and performing their own experiments. However, many of these reports have not dealt in sufficient depth with the considerable difficulties attendant on this type of experiment. In general, there is a large class of phenomena that can mask the sought-after effect and produce spurious or artefactual results which are actually due to prosaic and mundane albeit subtle phenomena. Some of the proposed experiments deal with superconductor-mediated detection of gravitational waves. These will not be dealt with specifically in this paper. Rather, we concentrate on those experiments designed to detect mass anomalies and gravity field anomalies. However, many of the issues raised herein are germane to both types of experiments. We will describe some general types of experiments concentrating on instrumentation and interpretation of results rather than the theory leading to the experiments. We examine specific and subtle thermal phenomena occurring during the transition of superconductors near T_{crit}. We then enumerate the multitude of experimental pitfalls that lay before the researcher. Examples provided clearly indicate that minimum standards of experimental precision, accounting for boundary conditions, an understanding of thermal exchange between cryogen and superconductor, error analysis and thorough reporting of the experiment are necessary to distinguish a true anomaly from prosaic explanations and artefacts.

Keywords: Gravitational forces, superconductors, high-Tc superconductors, low-Tc superconductors, type-II superconductors, superconductors cool-down, weight anomalies, gravity field anomalies, thermal exchanges in superconductors, error analysis, artefacts in gravitational experiments, gravity-like fields.

1. INTRODUCTION

This paper presents a brief analysis of experiments designed to confirm or reject claimed gravitational anomalies. We will not discuss conditions under which true anomalies possibly could arise nor the theoretical underpinning of such experiments but highlight detection methods and suggest some standards for their detection should they exist. We mainly focus on experiments involving liquid cryogen-cooled high-temperature superconductors (HTSC).

These experiments can be divided roughly into two groups: 1) experiments to determine mass anomalies assuming constant gravity ([1, 2]), and 2) experiments investigating gravity anomalies assuming constant mass [3, 4]. Weight anomalies are claimed to be either due to an intrinsic *materials* property (group 1) or that HTSC materials induced local variations in the *gravity field* (group 2). Experiments designed to produce or detect gravitational waves involving HTSC will not be discussed. Other papers in this eBook address gravitational waves. Here we focus primarily on force detection.

2. MASS ANOMALIES

Group 1 experiments can be subdivided into two classes: measurement of total weight of the complete experimental set-up; an indirect method that requires very large corrections to the data and compared to other approaches is more or less useless (*e.g.,* Fig. **1**) or direct detection of apparent weight of just the sample (plus suspension & fixtures-*e.g.,* Fig. **2**).

***Address correspondence to George Hathaway:** Hathaway Consulting Services, 1080 19th Sideroad, King City, Ontario, Canada L7B 1K5; Tel: 905-795-9382; Email: ghathaway@ieee.org

Giovanni Modanese and Glen A. Robertson (Eds)

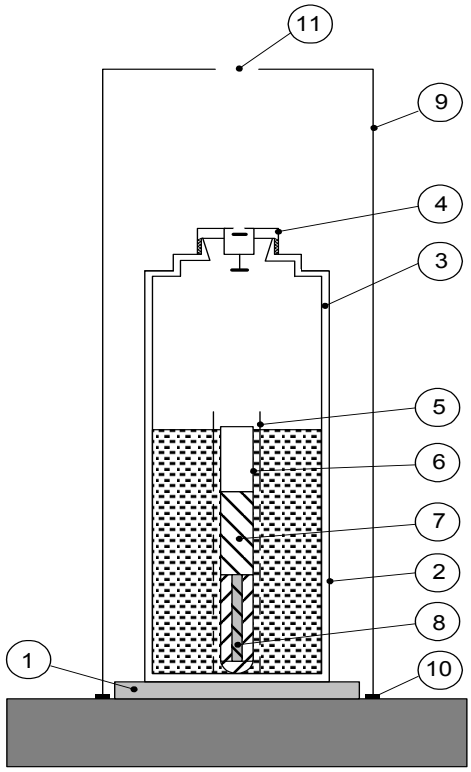

Figure 1: Set-up for measurement of total apparatus weight (Example of a low cost but completely unqualified set-up for gravity experiments); (1) Balance, (2) Stainless steel dewar, (3) Dewar insulation, (4) Plastic cap, (5) Cylindrical cavity, (6) Sample holder, (7) Glass fibre insulation, (8) Sample, (9) Hood, (10) Rubber seal, (11) Vent.

2.1. Detection of Sample Mass from Apparent Total Weight of Experimental Set-Up

Instead of directly measuring apparent weight of the sample, measurements of total weight of sample plus cryostat and coolant all positioned on an appropriate, mechanically stable balance could be performed (Fig **1**). As an advantage, no buoyancy or free convection or surface roughness or wetting phenomena have to be taken into account. However, substantial quantities of the coolant are evaporated when the sample is dipped into the liquid whilst suspended on a filament. Contrary to similar methods employing liquid cryogens where uncertainties in the height of the liquid result in very small buoyancy effects experienced by the thin filament, here the reduction of the liquid level results in a strong and fluctuating decrease of total weight. The liquid level cannot accurately be controlled and restored to the original height at $t = t_0$. A continuous, compensating supply of liquid to the cryostat would seriously disturb weight measurement. Liquid level height determines local temperatures on the inner wall of the cryostat and thus local heat flow through the cryostat's super-insulation Thus the evaporation rate of the coolant is not constant, masking the weight anomaly.

To avoid explosions, such measurements have to be taken in open atmosphere. This means condensation of water vapour and ice formation, this time not on a thin filament but on parts of the cryostat close to the neck, with much larger dimensions than a thin filament and correspondingly more condensate. In summary, from a thermal design standpoint, measuring of total weight of an experimental set-up is not recommended and data achieved in this way would likely be of little value.

2.2. Direct Detection of Sample Mass

There are four experimental criteria that provide the preferred means of direct detection of sample mass at cryogenic temperatures: (a) the sample is cooled solely by radiative exchange with a cold external heat sink, (b) the weight measurement is performed in vacuum, (c) sample weight data are taken using a magnetic suspension balance, (d) sample temperature is continuously monitored. If these conditions are

met, there is neither buoyancy in a fluid or gas nor sample wetting by a cooling liquid. Radiative cooling can be realised by allowing the sample to radiate away its heat to cryogenically-cooled surroundings through the vacuum. However in this case, cool-down can be very slow.

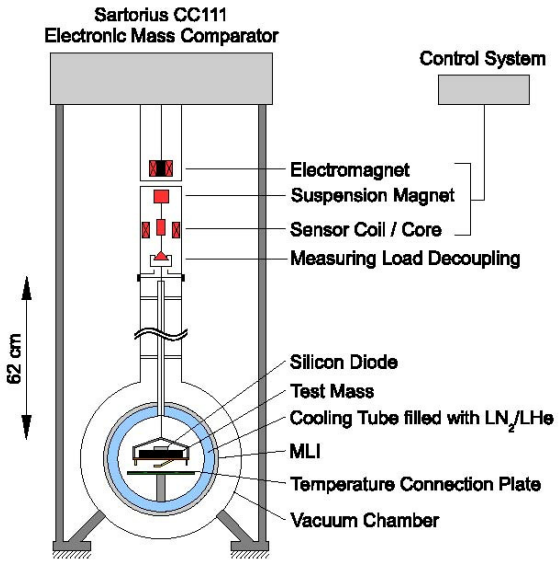

Figure 2: A superior experimental set-up for *Direct* Detectionof Sample Weight after Tajmar. Reprinted by Permission of *Meas. Sci. Tech.*, 21 (2010) 015111.

If radiative cooling through a vacuum is insufficient and cooling must occur by direct physical contact between the sample and a "cold head", weight and usually temperature data can be taken only at discrete times during non-contact, at which time the sample is warming up, hopefully at a well-defined rate. Note that a weight anomaly might occur just during contact, when the sample is coldest, and thus be missed. This is a particular problem when T_{crit} is close to the cryogen boiling point as with liquid nitrogen. This cooling method not only requires an interruption of the thermal contact between sample and cold head during data acquisition, but during contact also induces temperature gradients over the surface and through the thickness. Temperature gradients can result in only partial phase changes of the HTSC material which could substantially reduce the amplitude of possibly existing weight anomalies.

If (a) and (b) cannot be met in their entirety, cool-down can be realized by introducing a heat transfer gas, *e.g.,* helium, into the evacuated space surrounding the sample, allowing the sample to cool down more rapidly than by radiative transfer. As a consequence, buoyancy reduces sample weight. Further, if there is a small amount of water vapour in addition to the transfer gas, condensation of water vapour onto the sample and support filament will lead to a steady increase of sample weight, and the flow of water vapour to the cold sample can in turn induce convection. Application of high precision suspension balances then would be useless, and conventional balances would have to be used. A possible solution is to quickly pump out the transfer gas immediately after cool-down. Pumping of large volumes of helium is time consuming and can allow the sample to warm up during pump down.

These problems can be mitigated somewhat by clever design of the weighing chamber. To enable weighing in vacuum, any heat transfer gas must be pumped out quickly, necessitating the use of a small volume and minimum distances between sample and surrounding cold sink. Accurate temperature measurement at reasonable cost require physical contact between a thermocouple or cryogenic diode and the outside world by means of conductive wires which conduct unwanted heat to the sample. Using an intermittent physical conductive contact permits the sample to be cooled and weighed between direct temperature measurement. This also allows the sample to be suspended by the thinnest, least thermally-conductive suspension fibre suitable for the job.

Tajmar [5] has designed and implemented such an improved scheme with which he was able to cool by a combination of radiation and conduction (liquid helium transfer gas) solid samples to near liquid helium temperatures, accurately measured, and perform sensitive weight measurements in vacuum whilst the balance was self-calibrating. The sample was placed on a small weighing platform and a temperature-measuring diode was thermally attached to the sample. The platform was suspended by a single suspension fibre to a magnetic suspension system all enclosed in a vacuum chamber (see Fig.**2**). The suspension system allowed the whole platform to be raised and lowered a few millimetres at pre-determined times, during which balance calibration took place. The wires from the diode were attached to connector pins protruding from the bottom of the sample platform which, then the platform was in the lowered position, contacted a fixed base plate with appropriately-placed electrical contacts leading to the temperature readout circuit. Surrounding but not touching the weighing platform was a tightly-wound copper tube through which liquid cryogen was circulated in order the cool the sample. Helium gas was leaked into the small insulated weighing chamber to cool the sample by conduction and then quickly pumped out to allow accurate weighing in vacuum.

Theoretically the only means of warming the sample in a pure vacuum (never actually reached in practice) is conduction down the suspension fibre and radiation from hotter regions of the chamber walls.

While the evacuated magnetic suspension balance itself, as a sensitive scientific apparatus no doubt provides an excellent potential for weight measurements, precise understanding of thermal boundary conditions for gravity experiments during cool-down or warm-up periods could become a problem in successfully competing with the high weighing accuracy provided by the balance. An example numerical analysis is presented in Section 2.3 in which, among other experiments, the warm-up period of Tajmar's experiment [5] was modelled by a numerical solution of Fourier's differential equation for the temperature field of samples and their surroundings. While [5] claims radiation as the sole heat transfer in this experiment, indications of thermal leakages other than radiation were found during the analysis (Section 2.3.4). We further draw the attention of experimenters to possible shortcomings of this or any other experimental set-up that are related to small Biot numbers which can have significant influence on the results. This potential conflict arises from a possible mismatch between relaxation times for the phonon and electron responses to thermal disturbances resulting during warm-up or cool-down periods. This effect will be addressed in Section 3.

The Tajmar set-up [5] involved an expensive magnetic suspension balance and considerable machine fabrication. For most experimenters this option may not be available so direct contact between liquid cryogen and sample may be the only alternative. Though this certainly reduces experimental effort and cost, the results may be of little use however. The setup shown in Fig. **1** is a striking example.

In these cases, additional problems arise if the sample is cooled by dipping in a boiling, cryogenic liquid and the liquid is then allowed to boil off, exposing the sample to cold vapours. Immediately after dipping of the sample at time t_0, into the liquid, strong boiling (due to the heat capacity of the sample) causes the sample which is usually hanging freely on a fibre to swing violently in the liquid for some minutes. During this period, sample weight anomalies can become completely obscured. After thermal equilibrium is achieved at time $t_1 >> t_0$ the data curves become smooth (Fig. **3**). The strong weight fluctuations immediately after dipping have little effect on the experimental results provided the height of the liquid is kept at approximately constant level and the HTSC material at $t = t_1$ has not already experienced a phase change. The time scale during which a phase change occurs can be analysed numerically if heat transfer at the liquid/solid interface and thermal diffusivity of the sample material are known (compare Section 2.3.3). While boiling and convective heat transfer involving various materials have been extensively studied in the literature, little information is available about heat transfer at the liquid/sample interface for HTSC materials. In these situations, a fit to experimental data would be necessary.

Heat transfer not only determines the temperature excursions of the sample but also the rate of free convection or two-phase (*i.e.,* gas bubble/liquid) flow in liquid layers close to the sample surface. Weight *vs.* time data taken from typical HTSC dipping experiments show the super-position of a variety of

contributions including rest mass of the sample, buoyancy, convection in the liquid, ejection of bubbles, temperature gradients and de-wetting. While buoyancy can be compensated to a greater or lesser extent, it can impose a significant error source if a sample holder housing the superconductor samples is used for the set-up and its material experiences phase transitions, with a corresponding uncontrollable change of volume of the sample holder. Usually de-wetting results in temperature gradients in the sample which cause a phase change to occur in slices rather than in the entire sample at once. No firm conclusions concerning existence or non-existence of a gravity anomaly can be taken from this type of data.

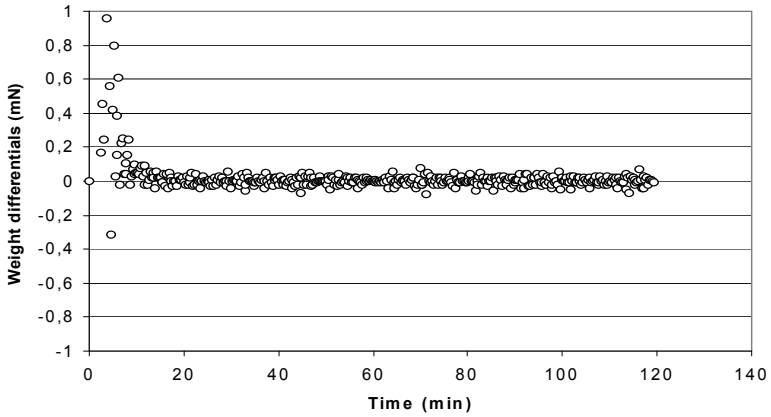

Figure 3: Weight Differentials (Apparent Weight Differences $AW(t_{N+1})$ - $AW(t_N)$) Between Single Data Points Taken at Discrete Time Steps $t_N < t_{N+1}$ Using a Pile of 10 YBaCuO Pellets in a Sample Holder that at t = 0 is Dipped into LN_2. Reprinted by Permission of *Physics Essays Publication*, from *Physics Essays*, 16, 236-253 (2003).

In the case of the sample being completely immersed in liquid for the duration of the experiment, "dummy" weights can be used as standards [1] that under no circumstances should undergo changes of their rest mass. Identical surface quality and heat transfer properties of the HTSC samples and dummy samples can be obtained by housing them in a sample holder made from a material such as PTFE (Teflon), whose thickness and material is selected to shift the phase change of the HTSC samples to times greater than t_1, but again there may be phase changes of the PTFE material which would uncontrollably alter buoyancy. It may also be possible to chemically treat the HTSC samples to be non-HTSC, eg by addition of a tiny quantity of Zn to the precursor powders, but otherwise identical.

2.3. Numerical Analysis of Warm-up and Cool-down Experiments

A numerical FE (finite element) analysis has been performed to obtain sample temperature evolution, T(x,y,z,t), under strongly differing heat transfer conditions in cool-down and warm-up experiments. In terms of thermal resistances to a liquid coolant (at 77 K) or to a radiative environment (at RT), temperature excursion of the HTSC pellets is analyzed with respect to four conditions, namely the following items (see also Fig. **4**):

1) **Cool-down**, with only liquid boiling/liquid convection at the sample/coolant interface; heat transfer is modeled with temperature dependent (and thus time-dependent) boiling and convection heat transfer coefficients at the interface to the coolant (resistance R1); there is no further thermal resistance between coolant and sample (Section 2.3.1),

2) **Warm-up**, with no liquid phase present but a convection resistance (R21) at the interface to ambient and, in series, a conductive resistance (R22, of a sample holder) between interface and sample (a weak radiation contribution is included in R22) (Section 2.3.2),

3) **Cool-down**, with conductive resistance between pellets and sample holder walls (R_{31}) and, in series, a liquid boiling/convection resistance (R_{32}) at the interface to the coolant (Section 2.3.3); the sample holder is the same as in item 2,

4) **Warm-up**, solely radiative heat transfer between sample and radiative environment, with solely a thermal radiation resistance (R4 only - no further resistance between environment and sample), with the sample exposed under vacuum. This part of the diagram schematically describes the inner heat transfer rates in the suspension balance experiment reported by [5] (Section 2.3.4).

The total thermal resistance increases from items (1) to (4).

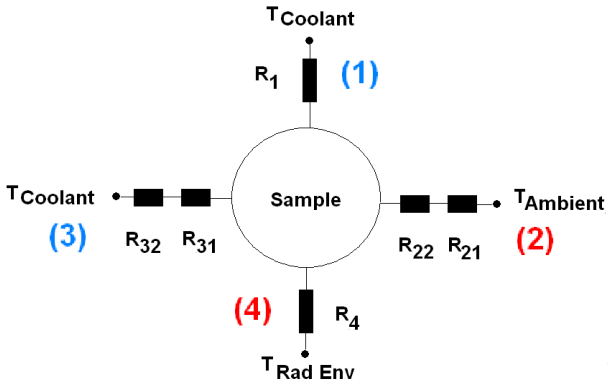

Figure 4: Thermal resistances (schematic) indicating the conditions under which finite element calculations for items (1) to (4) were performed. Indices of the individual resistances, R_{kl}, are assigned according to direction of heat flow (hot to cold).

2.3.1. Cool-down Experiment (Simulation of the Meissner-Ochsenfeld effect)

Previously [6], we reported on the time dependence of the Meissner-Ochsenfeld effect. Numerical analysis shows that it takes a superconductor pellet after start of cool-down a time interval, Δt, in the order of tens of seconds, depending on the anisotropy of its diffusivity, to get a sufficient number of volume elements, N_{SC}, superconducting (Fig. **5**); otherwise there is no stable levitation position where total levitation force balances gravity. In this analysis the size of each of the N volume elements was 200 x 200 x 20 μm^3 for simulation of a polycrystalline YBCO material (because of cylindrical symmetry and under mapped meshing, the number of finite elements is different from N).

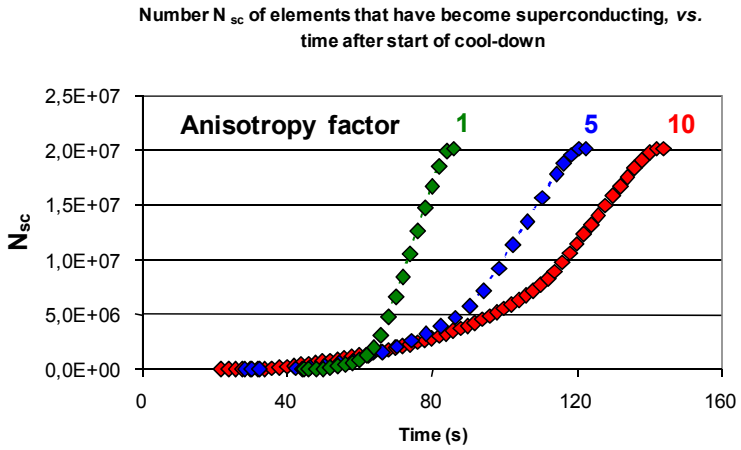

Figure 5: Number $N_{sc}(t)$ of elements for 3 different anisotropy ratios of thermal conductivity (see text) that have become superconducting, *vs.* time after start of cool-down. The curves are calculated from numerical (finite element) results for the temperature profiles T(x,y,z,t) during the cool-down period of a YBCO pellet. The figure shows part of the data reported in *Cryogenics* 49 (2009) 433-448.

The sample is directly wetted by LN_2, with no thermal resistance other than from boiling and convection between coolant and sample surface. Results of the simulations compared well with levitation experiments using a YBCO pellet of exactly the size as simulated in the finite element calculations (the calculated time for obtaining a stable levitation position was indeed confirmed in the experiment). This in turn confirmed that simulation of the external heat transfer (violent boiling followed by liquid convection during field cooling) was adequate.

2.3.2. Warm-up Experiment using small YBCO Pellets in a Sample Holder

This the reverse of the cool-down (dipping) experiment reported in [1] (the corresponding numerical analysis of the cool-down period is described in the next Subsection). In the present case, warm-up was in ambient atmosphere. Comparison of the considerably longer time needed for the sample to arrive at room temperature was roughly confirmed by the calculations although extrapolations were made, since extending the simulation to very long time intervals consumes much computer time. External heat transfer was by convection in natural atmosphere and by radiation to the warm environment using heat transfer coefficients from standard texts.

Fig. **8** (red full and open diamonds and squares) shows derivatives dT/dt of pellet temperature at positions on top and bottom of the pile of 18 pellets, respectively.

2.3.3. Cool-down Experiment using small YBCO Pellets in a Sample Holder

In this experiment, samples (pellets) were housed in a cylindrical sample holder. We will not comment on tentative conclusions from the unexplained observation of a weight increase of the pellets but simply analyse the thermal aspects of the experimental setup as an example where a large thermal resistance represents the interface between the coolant and samples.

Since [5] designed a replication experiment, it is worthwhile to emphasize the difference between the experiments reported in [1, 5]: Tajmar measured weight dependence on temperature of a single pellet under vacuum, in zero applied magnetic field and during *warm-up*, with no buoyancy effects to be compensated. Temperature distribution in pellet and cavity is almost perfectly homogeneous, due to the weak external heat transfer (although it was not solely radiative, see Section 2.3.4). Transition of the whole pellet volume, from superconducting to normal state, is *sharp in time* (overall warm-up rate is rather quick). The dipping experiment [1], on the other hand, used a sample holder that had an internal cavity housing up to 18 small YBCO or BSCCO pellet partly in a local external magnetic field, with the sample holder dipped into liquid nitrogen, *i.e.,* the measurement was done during *cool-down* and with buoyancy in the liquid that had to be compensated. Heat transfer from the inner wall of the sample holder to the pellets is much stronger than under radiation heat transfer, though the strong heat transfer fluctuations (violent boiling, followed later by convection) at the outer sample holder surface is damped by the thermal resistance of the PTFE wall. This means cool-down proceeds fast, and there will be strong, non-vanishing radial temperature gradients in the pellets. Transition from normal to superconducting state in the pellet volume accordingly will be *gradual in time.*

Overall design of sample holder and an internal cavity is shown in Fig. **4** of [1] with a detailed description not repeated here. Cool-down of the sample holder is described by heat transfer coefficients, α, for boiling and convection under liquid nitrogen. We used the same α-values reported in [6], where the heat transfer coefficients, although obtained from the literature from measurements on a metallic surface, were confirmed by levitation experiments. The thermal resistance and heat capacity of the walls of the sample holder serve to shift a possibly-existing weight change during phase transition to a time after which the initial violent movements of liquid and sample holder under boiling will have ceased.

Temperature evolution during cool-down and radial temperature gradients are illustrated as a contour diagram in Fig. **6**. Transition of the HRSC pellets (red) from normal to superconducting state has not started until well after 60 s, and is not accomplished until after t = 720 s after start of cool-down (see Fig. **7**).

Fig. **8** (blue full and open diamonds and squares) shows derivatives dT/dt of pellet temperature at positions on top and bottom of the pile of 18 pellets, respectively. Also shown is the dT/dt derivative of the purely radiative heating condition of item 4 (black circles). The derivatives dT/dt of the cool-down experiment (item 3) are orders of magnitude larger than the values calculated for the suspension balance experiment (radiative heating, item 4).

Radial temperature differences in the pellets in the cool-down (item 3) experiment shown in Fig. **9** are quite large due to conductive thermal resistance introduced by the wall of the sample holder and also a few thin layers of glass fibre paper between sample holder and pellets.

Figure 6: Temperature distribution in the sample holder used in the cool-down (dipping) experiment reported in [1] calculated at t = 60 s after start of cool-down under boiling and convection in LN_2. For details of geometry of sample holder and superconducting pellets housed in an internal cavity see [1].

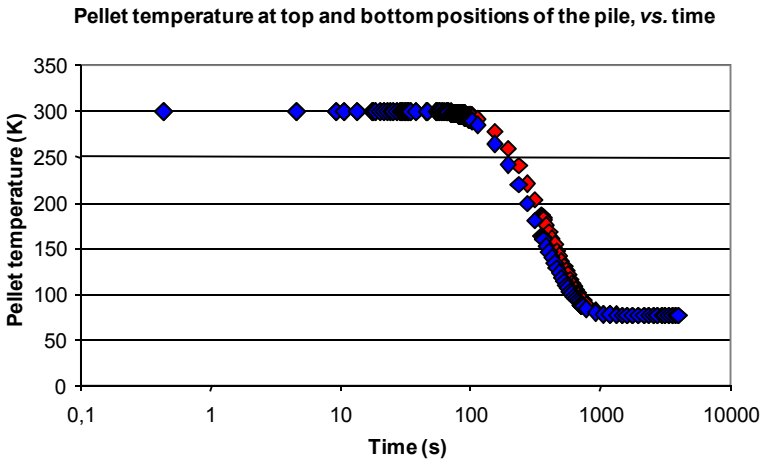

Figure 7: Pellet temperature evolution calculated at central pellet positions for the uppermost (red diamonds) and lowermost pellets (blue diamonds) of the pile consisting of in total 18 YBCO pellets in the experiment reported in [1] *vs.* time after start of cool-down.

We also compared calculated temperature evolution in the case where the pellets were replaced by ceramic powder in the cavity with the temperature measurement reported in Fig. **8** of [1]. There, T = 77 K is reached in the cavity after about t = 300 s. This is roughly confirmed by the numerical simulation if we assume an uncertainty between 0.1 to 1 K of the temperature measurement using a Pt-100 thermometer. The same heat transfer coefficients for cooling with LN_2 have been applied as before thus confirming the validity of the set of α-values prepared in [6] from the literature.

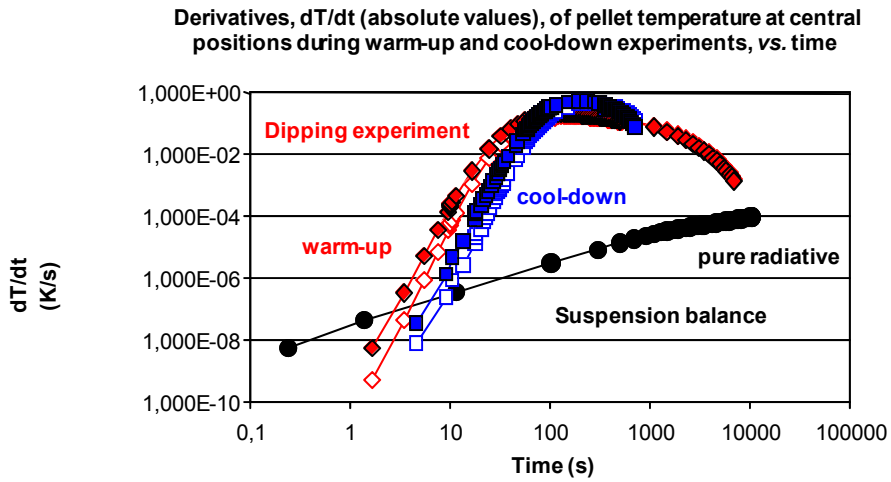

Figure 8: Derivatives, dT/dt (absolute values), of pellet temperature at central positions of pellet during warm-up and cool-down periods in suspension balance (black circles, pure radiative heat transfer) and dipping experiments (full and open diamonds and squares, for the dT/dt at top and bottom positions of the pile, respectively), *vs.* time.

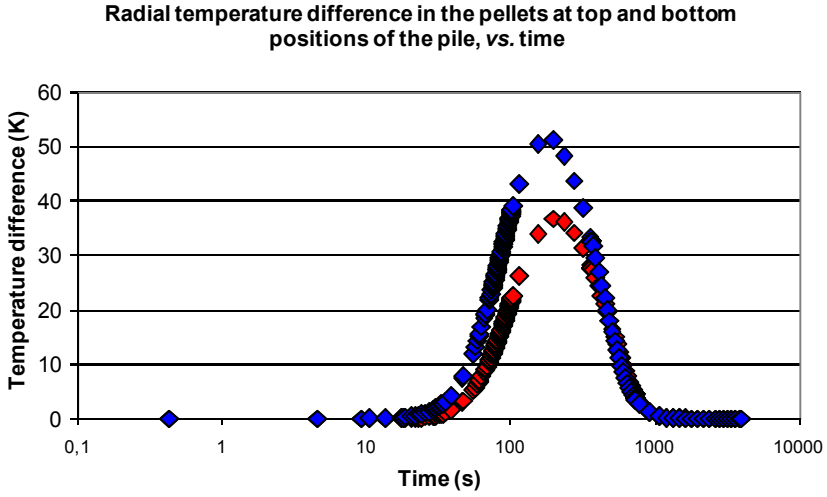

Figure 9: Radial temperature differences for pellet temperature evolution calculated at central pellet positions for the uppermost (red diamonds) and lowermost pellets (blue diamonds) of the pile consisting of in total 18 YBCO pellets, *vs.* time after start of cool-down.

2.3.4. Warm-up Experiment using a YBCO Pellet in a Suspension Balance

As above, we will not comment on the interpretation of the results of the experiment reported by Tajmar [5]. Tajmar's innovative setup is used simply as an example, in this case for the high radiative resistance between YBCO pellets and a radiative environment the temperature of which increases slowly during warm-up from cryogenic to room temperature.

This experiment, essentially an attempt to replicate the "dipping" experiment described in the previous subsection (item 3), applies pure radiation heat transfer to a superconducting pellet. The authors [5] correctly claim that weak external heat transfer (like radiation exchange) in relation to much stronger (conductive) internal heat transfer, reflected in a small Biot number, is responsible for uniform temperature evolution in the sample, which means all volume elements of the sample pellet will arrive at critical temperature at almost the same time after start of warm-up.

While application of Equations. (2) to (5) in [5] was made to quantify this expectation, these equations are valid under static conditions only. But it was correct when the authors more intuitively assumed that sample temperature evolution was uniform. The phase transition in the whole sample volume accordingly is completed instantaneously which means a very large decay rate of electron pairs to quasi-particles will be required to satisfy the phonon aspect of evolution of the disturbance (this aspect will be addressed in Section 3). But from an initial viewpoint, experiments [1, 5] cannot be declared identical, or item (4) a replication of item (3), simply from thermal boundary and internal heat transfer considerations. Contrary to a statement made in [2] (a first attempt made by the same authors to replicate the dipping experiment), the dipping (cool-down) experiment reported in [1] was *not* performed in gaseous but solely under *liquid* nitrogen, and most of the error analysis in [1] had to account for exactly this problem.

In the present analysis, we simulate the neighbourhood of the pellet by two concentric cavities with closed ends. Tajmar [5] reports length and inner radius of the cavity is 92 and 25 mm, respectively. To provide an upper limit of the derivative, dT_{Cav}/dt, of cavity temperature, T_{Cav}, we assume that the cavity has a wall thickness of 2 mm; increased thickness would increase thermal mass of the cavity und thus reduce dT_{Cav}/dt.

For the simulation, we use a thermal emissivity, ε_{ML} = of 0.0315 at cryogenic temperatures, of 30 metallized Mylar foils. For this ε_{ML} see [7] and references cited therein. The simulated sample is a $YBa_2Cu_3O_{7-\delta}$ (YBCO) pellet of 12.5 mm radius and 3 mm thickness. During warm-up, the YBCO pellet is freely hanging inside the cavity. In the experiment, the pellet is connected to the suspension balance by a single thin V2A-wire of 0.125 mm radius and of 62 cm length. In the simulation, the wire near the pellet surface is split into 3 more wires (to avoid meshing problems that would arise near a centrally located point of contact), each with the same radius as before, and the 3 wires are attached to a sample holder that consists of a 0.5 mm thick plate of radius 12.5 mm (same as pellet radius, an assumption with no effect on the results). Pellet and sample holder are positioned 3 mm above a connecting plate of 15 mm radius that besides radiative heat exchange is thermally coupled to the cavity wall by a conducting solid support column of 1 mm radius. Cavity, sample holder, connecting plate and column are all made of Cu. It should be emphasized that (but small, if any) deviations of the simulated experimental setup from the real laboratory setup do not have any significant influence on the simulation results.

Thermal conductivity, λ, and specific heat, c_p, of YBCO and Cu used in the simulations are the same as reported in [6]. Anisotropy of thermal conductivity of YBCO is accounted for again by the ratio $\lambda_{ab}/\lambda_c = 10$ in the ab-plane and c-axis direction. The emissivity, ε_{SC}, of the YBCO pellet and the ε_{Cu} of copper are about 0.9 and 0.1, respectively. The ε_{Cu} is taken from [8] for cryogenic temperatures, but little information is available for the emissivity of YBCO, especially in the SC state. We use the value $\varepsilon_{SC} = 0.9$ which is typical for ceramics (YBCO in the normal conducting state) in the interval between cryogenic to low temperatures, [9]. All emissivities, ε, used in this paper are hemispherical total values.

2.3.4.1. Radiative Energy Balance (Analytical Expressions)

Radiative heat transfer through the multi-foil super-insulation, in cylindrical geometry, is calculated in two steps: The first step involves the relation for radiative transfer between two concentric, infinitely extended cylinders with surfaces A_1 and A_2 and with no foils in-between. Here the outer surface, A_2, constitutes the environment outside the cavity (a vacuum chamber made of V2A stainless steel fixed into the suspension balance). The inner surface, A_1, is the cavity wall. The V2A steel wall of the vacuum chamber is at T_2 = 300 K (constant), while the intervening cavity wall is at transient temperature $T_{Cav} = T_1 = T_1(t)$ during warm-up. With ε_{V2A} indicating the emissivity of the vacuum chamber and σ the Stefan-Boltzmann constant, we have the well-known relation for heat flow:

$$Q_{Rad,0}(t) = -\sigma A_1 (T_{Cav}^4 - T_2^4)/[1/\varepsilon_{Cu} + (A_1/A_2)(1/\varepsilon_{V2A} - 1)], \quad \textbf{(1a)}$$

see *e.g.*, [10]. All surfaces are assumed as grey diffuse radiators, and all $Q_{Rad}(t)$ in Eqs. (1) to (3) are given in W. The minus sign in Equation (1a) accounts for a positive radiative heat flow from the environment A_2 to surface A_1 during warm-up of the sample.

Second, we use the "shielding efficiency", ζ, of evacuated multi-layers [11] to reduce $Q_{Rad,0}(t)$ from Equation (1a) to

$$Q_{Rad}(t) = \zeta\, Q_{Rad,0}(t) \quad \textbf{(1b)}$$

with

$$\zeta = \{1+(\eta_{Cav}/\eta_{ML})\, r_1 \sum 1/[r_1+(n/(N+1))(r_2-r_1)]\}^{-1} \quad \textbf{(1c)}$$

in cylindrical geometry. The dimensions of the cavity require application of Equation (1a-c), and by no means would the result be correct if one would erroneously apply corresponding expressions for plane-parallel walls.

In Equation (1c) we use N = 30 the number of foils, and the summation is taken over $1 \leq n \leq N$. In this equation, η_{Cav} and η_{MF} denote reduced (dimensionless) emissivity, $\eta_{Cav} = \varepsilon_{Cu}/(2-\varepsilon_{Cu})$ and $\eta_{ML} = \varepsilon_{ML}/(2-\varepsilon_{ML})$, respectively, and r_1, r_2 the radii of surfaces A_1 and A_2 (r_1 = 25, r_2 = 250 mm). For simplicity, we have assumed $\varepsilon_{Cu} = \varepsilon_{V2A,}$ at cryogenic temperatures.

The residual error contained in Equation (1b,c), *i.e.,* neglecting the end surfaces, will be compensated by the finite element model described in the next Subsection. Division of $Q_{Rad}(t)$ by A_1 and the temperature difference

$$\Delta T(t) = T_2 - T_{Cav}(t) \quad \textbf{(2a)}$$

between ambient and cavity yields a transient heat transfer coefficient

$$\alpha_{Rad}(t) = Q_{Rad}(t)/[\, A_1\, \Delta T(t)] \quad \textbf{(2b)}$$

for radiative exchange between ambient (the vacuum chamber) and the outer wall of the cavity. As for many evacuated super-insulations, the α_{Rad} are very small, below 2 W/m^2. Under transient conditions, heat flow $Q_{Rad}(t)$ through the super-insulation onto the cavity wall splits into

a) Radiation (emitted or reflected, because all $\varepsilon < 1$) that is distributed internally, *i.e.*, from the cavity inner wall to sample, sample holder, connecting plate and support column,

b) Thermal conduction that distributes heat also in the cavity wall according to its heat capacity.

In the subsequent energy balances, and in all numerical simulations reported in the next Subsection, temperature dependent quantities (density, specific heat, thermal conductivity as in [6]) have been applied.

Assume tentatively for the moment, and as a first order of magnitude estimate, that there will be *no* radiation exchange inside the cavity. This yields an upper limit for the rate of change of (medium) cavity temperature

$$dT_{Cav}/dt \leq Q_{Rad}(t)/(V_{Cav}\, \rho_{Cav}\, c_{Cav})\ [K/s] \quad \textbf{(3)}$$

with V_{Cav} the volume and ρ_{Cav} and c_{Cav} density and specific heat of the cavity walls at cryogenic temperatures, respectively.

Fig. **10** (solid diamonds) shows dT_{Cav}/dt calculated from Equation (3) from which we can roughly estimate the period of time, $\Delta t'$, needed for the cavity with *no* radiation exchange inside, to arrive at T = 160 K (the value indicated in Fig. **4** of [5] after about 3 hrs into the warm-up period),

$$\Delta t'[(T_{Cav}(t)] = [T_{Cav}(t=3\ hrs).T_{Cav}(t=0)]/\ dT_{Cav}/dt \quad \textbf{(4)}$$

Since the rates dT_{Cav}/dt decrease with increasing time, we will take dT_{Cav}/dt at 120 K (about 5.6 10^{-4} K/s) from Fig. **10** as an average value. This yields $\Delta t'[(T_{Cav}(t)]$ of about 41 hrs instead of the 3 hrs indicated in Fig. **4** of [5], which strongly suggests that radiation was not the *sole* heat transfer mechanism when the experiment was performed. Obviously, pure radiative heat transfer would be too weak to confirm the temperature increase to the claimed 160 K.

For a second, again order of magnitude estimate with the same analytical model, assume that the same thermal power, $Q_{Rad}(t)$ from Equation (1a-c), is delivered to the *whole* assembly (cavity plus the inner components like sample, sample holder *etc.*). We will take dT_{all}/dt at 85 K (about 7.2 10^{-4} K/s), again from Fig. **10** (solid squares), to estimate $\Delta t'[(T_{all}(t)]$. This would take all components about 6 hrs to reach the critical temperature, T_{crit} = 92 K, of standard YBCO, still definitely longer than the 3 hrs indicated in Fig. **4** of [5]. After this period of time, the cavity temperature necessarily is at 92 K (the evacuated multi-foils act like a thermal mirror), not at the claimed 160 K. This is also a natural consequence of the isotropic temperature distribution occurring in a cavity furnished with evacuated thermal super-insulation, under static or as is the case here, under quasi-static conditions. Already these comparatively simple but obvious energy balances deliver results for the expected temperature evolution that are in clear contrast to what is reported in [5].

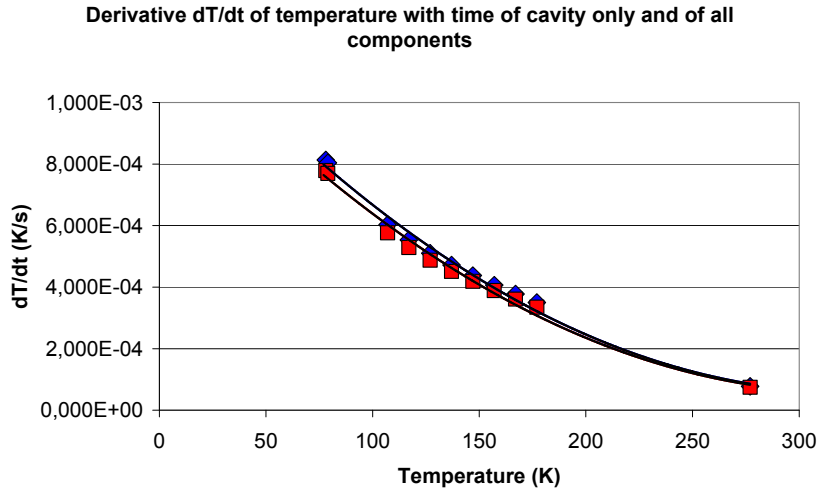

Figure 10: Derivatives w.r.t. time, dT_{Cav}/dt and dT_{all}/dt, of temperature of cavity (red squares) and temperature of the whole assembly (blue diamonds that for cavity plus pellet, sample holder *etc.* almost coincide) used in the warm-up (suspension balance) experiment reported in [5] *vs.* cavity temperature (all data are mean values).

It makes no difference for these analytical order of magnitude-estimates whether a YBCO sample or a Cu-pellet is introduced into the cavity, and all these expectations are confirmed in the numerical modelling described in the next Subsection.

2.3.4.2. Numerical Modelling

A standard finite element (FE) program and mapped meshing was applied to YBCO-pellet, sample holder and connecting plate, while free meshing was allowed for the cavity including its end faces. The four wires connecting the sample holder to the balance, and the column to support the connecting plate, were modelled with 1D-thermal elements. For all other components, 3D-solid elements were used. Radiation heat transfer inside the cavity was modelled with 2D-surface elements using radiation exchange factors, the different emissivity of all components, and a radiation matrix element that incorporates all these data and the corresponding view factors in-between.

The calculated temperature excursions successfully reproduced not only experimental surface temperature excursions, but the results are also in very good agreement with levitation experiments performed by one of the authors (H. R.). Both observations confirm the heat transfer simulations made in the FE simulations of the four experiments (items 1-4). In particular, the FE analysis provides a look into the *interior* of the sample and the thermal relaxation time.

As in the previous Subsection, neither cavity nor sample temperature claimed in Fig. **4** of [5] can be confirmed by the results of the numerical simulations at a time 3 hrs after start of the warm-up period if we assume solely radiative heat flow from the vacuum chamber to the cavity. Instead, an effective, external heat transfer coefficient not confined to radiation exchange had to be defined to speed up temperature increase so as to conform to the data measured by Tajmar. Calculations started at T = 77 K and were uniform for cavity, sample and sample holder, connecting plate, column and wires. The end of the long wire that connects the sample holder to the suspension balance was kept at 300 K constant.

The effective heat transfer coefficient describes *external* heat transfer, *i.e.,* from ambient, that is,. the vacuum chamber, to the cavity only, while *internal* heat transfer, *within* the cavity, is *solely* by radiation. A realistic external heat transfer coefficient may result from a variety of heat leakages like solid/solid contacts through the super-insulation, or from non-insulated parts of the assembly, or from residual gas pressure that was not sufficiently removed before and during the warm-up experiment (note the strong fluctuations of gas pressure seen in Fig. **4** of [5]). Various constant values of the effective heat transfer coefficient were then assumed in the numerical calculations (α_{eff} = 0.1, 0.25 and 1 W/(m^{2}K)). For comparison, a hypothetical free air convection around a horizontal cylinder was modelled using the relations reported in [12]. Free convection α-values for ambient air, under this geometry, amount to about 10 W/(m^{2}K), which, as can be seen, is certainly too large. Another option was to assign α_{eff} = 0.1 W/(m^{2}K) to regions near the ends of the cavity and 0.25 W/(m^{2}K) to its central parts (indicated by "0.1/0.25" in the following figures).

Fig. **11a** and **b** shows numerically calculated cavity and pellet temperature *vs.* time for various values of the effective heat transfer coefficient. Comparison with the *cavity* temperature reported in Fig. **4** of [5] shows that after t = 3 hrs the curve calculated with α_{eff} = 0.25 W/(m^{2}K) provides the best approximation to the reported data, while comparison of calculated *pellet* temperature with the value (about 95 K) reported from the measurements is best when using α_{eff} = 0.1 W/(m^{2}K). It is again obvious, now from Fig. **11a** and **b**, that *solely* radiative heat flow to the cavity explains neither pellet nor cavity temperature evolutions reported in Fig. **4** of [5].

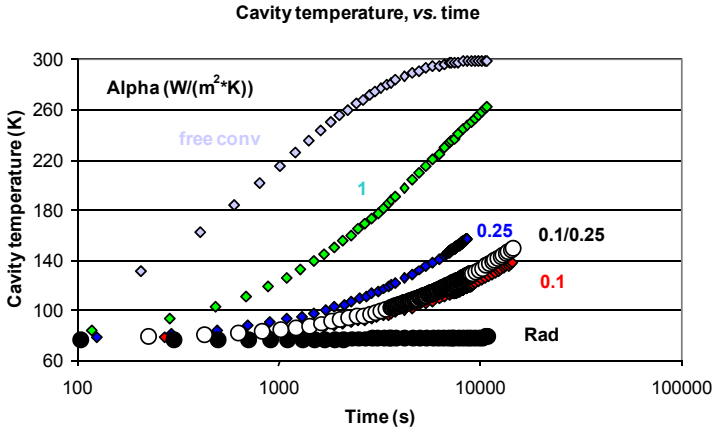

Figure 11a: Calculated cavity temperature evolution *vs.* time, for the warm-up (suspension balance) experiment. Data come from the finite element model with different values of the effective external heat transfer coefficient, α, describing heat exchange either solely by radiation ('Rad') between vacuum chamber and cavity through multilayer super-insulation, of using effective α-values (0.1 to 1 W/(m^{2}K)). Also shown for comparison is free convection of ambient air surrounding a horizontal cylinder. The α-value incorporates possibly existing heat leakages and is adjusted to reproduce the temperature evaluation reported in [5]. The '0.1/0.25' curve refers to α-values of 0.1 and 0.25 W/(m^{2}K) applied at the end and central sections of the cavity, respectively.

Fig. **12** shows temperature distribution on the upper surface of the pellet obtained for purely radiative heat flow soon after the start of warm-up. At cryogenic temperature, radiative heat transfer is weak as in the experiment in [5] but even temperature disturbances caused by the 3 thin wires attached to the sample holder can be made visible on the pellet surface (compare the temperature scales indicated in the figure). As was to be expected, the temperature distribution on the pellet is very homogeneous, within few 10^{-3} K, for all heat transfer options tested for simulation of this experiment and confirms the expectation (temperature homogeneity) in [5].

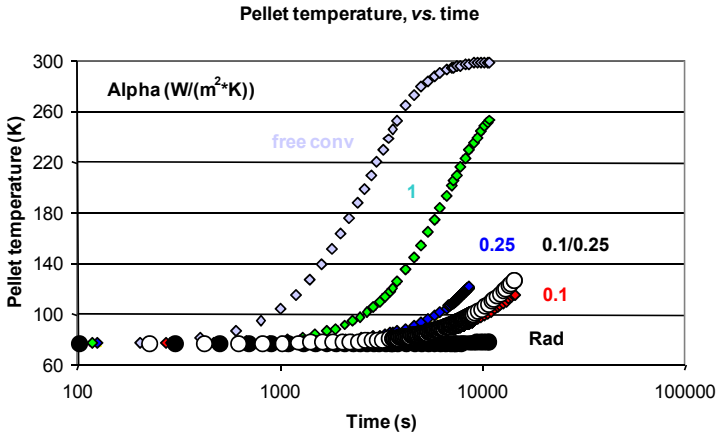

Figure 11b: Calculated pellet temperature evolution *vs.* time in the warm-up (suspension balance) experiment reported in [5]; results are given for different values of the external heat transfer coefficient, α (same as in Fig. **11a**). For details see text.

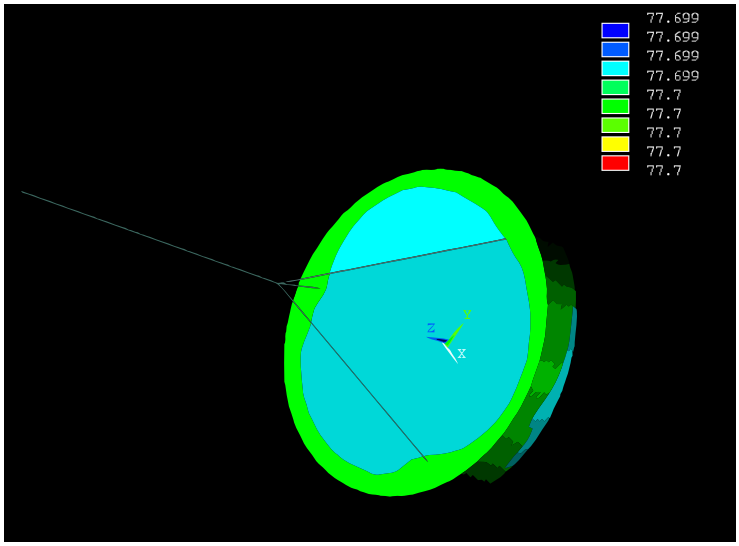

Figure 12: Temperature distribution on the upper surface of pellet soon after start of the warm-up period in the suspension balance experiment reported in [5] calculated for solely radiative external heat transfer. The thin lines indicate the 1D-elements used for the 4 thin wires that attach the sample holder to the balance. The xyz-triad located at the origin of the pellet is given for orientation (the co-ordinate z points in vertical direction).

Pellet and cavity surface temperature distribution is given in Fig. **13a** and **b** for the pellet at a time immediately before the phase transition at 92 K. At the phase transition, there are almost no radial temperature gradients in the pellet.

With the same volume elements as before (width and length of 200 μm but 50 μm thickness), we have about N = 7.3 10^5 elements in the pellet volume of 25 mm diameter and 3 mm thickness. Counting the

number $N_{SC}(t)$ of elements with temperatures $T < T_{crit}$ then yields the curves given in Fig. **14**. As is to be expected from the very homogenous temperature distributions in the pellet, the transition from superconducting to normal conducting state is very sharp for this condition ("warm-up 4"). The curve falls within a Δt of 4 s from the first to all elements becoming normal conducting.

Note in Fig. **14** that the temperature interval, ΔT, between start temperature in the experiments and phase transition is between 77 K and T_{Crit} in the warm-up experiments (ΔT about 15 K) while it is between RT and T_{Crit} during cool-down (ΔT almost 210 K), respectively. Together with the thermal resistances in the pellets and those at the interface to the coolant or to radiative environment, this explains the location (in time) of the phase transition (saturation of the curves at maximum $N_{SC}(t)$ during cool-down, or at $N_{SC}(t) = 0$ during warm-up, respectively). The shift observed from curve (1) to curve (3) results from the additional conductive resistance in (3), and the corresponding shift from (2) to (4) is due to a very large radiative resistance in the suspension balance experiment (4).

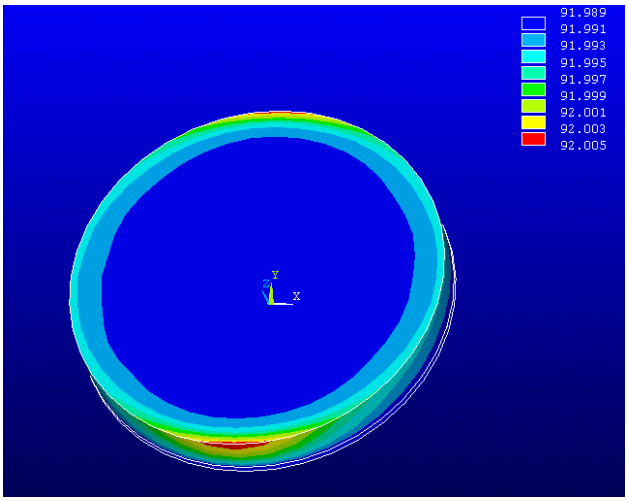

Figure 13a: Temperature distribution on upper surface of pellet calculated for the external heat transfer coefficients, α = 0.1 and 0.25 W/(m^2K) applied to the end and central sections of the cavity, respectively, at t = 7120 s after start of warm-up phase in the suspension balance experiment reported in [5]. Data are given in the immediate neighbourhood of the superconductor/normal phase transition. The xyz-triad located at the pellet origin is given for orientation.

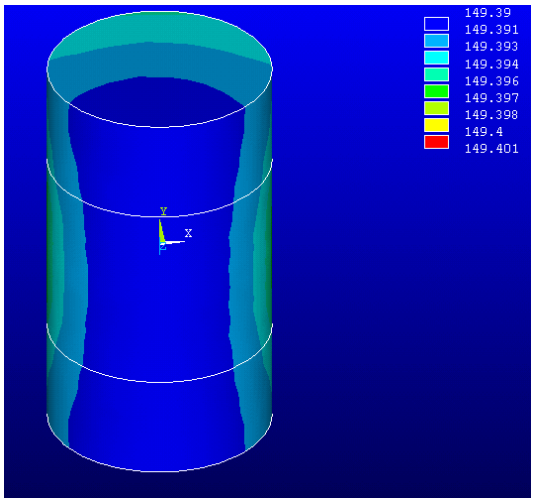

Figure 13b: Cavity surface temperature distribution (with closed ends) calculated for the external heat transfer coefficients, α = 0.1 and 0.25 W/(m^2K) applied to the end and central sections of the cavity, respectively, at t = 4 hrs after start of warm-up phase in the suspension balance experiment reported in [5]. The xyz-triad located at the pellet origin is given for orientation.

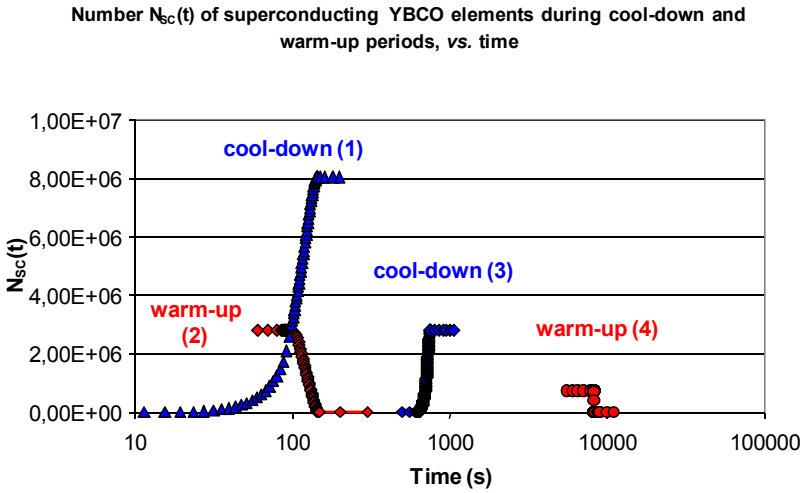

Figure 14: Number $N_{SC}(t)$ of superconducting (SC) of a total of N volume elements (width and length each 200 μm, thickness 50 μm) in the cool-down and warm-up experiments (items 1 to 4) for the finite element simulation of temperature excursion of polycrystalline YBCO pellet material *vs.* time, to identify the location (in time) of the phase transition after start of cool-down. See Fig. **4** for identification of the corresponding thermal resistances.

2.3.4.3. Summary of Section 2.3.4.

We have confirmed the expectation made in [5] that sample temperature evolution would be highly uniform during the warm-up period of item (4). It appears that either radiation was not the sole heat transfer mechanism in the suspension balance experiment, or else radiative heat transfer was rather non-uniform outside and inside the cavity. This situation might be improved if measures are taken against obviously existing thermal leakage. On the other hand, measures like these would hardly change the dT(t)/dt of the pellet, and the principal question is whether it is really an advantage in a gravity experiment of group 1 of the above to obtain a *sharp* superconductor/normal conductor phase transition of the whole sample (see next Section).

3. LIFETIMES OF THERMAL EXCITATIONS

An aspect that may become important for any of the experiments mentioned in the previous sections covers a possible mismatch between relaxation times of

a) Propagation of a thermal disturbance by conduction in a superconductor sample during cool-down or warm-up experiments, and

b) The response of the electron system of the superconductor to the same disturbance.

3.1. Two Competing Relaxation Times

Thermal diffusivity determines a characteristic time, τ_{Ph}, for propagation of thermal waves in solids after a thermal excitation. At very low temperature the superconducting electronic system is decoupled from propagation of thermal waves but reflects its own dynamic response to this or other specific excitations by corresponding relaxation times, τ_{El}. Both relaxation times, τ_{Ph} and τ_{El}, to the same disturbance (in the present case, a temperature increase or decrease) are not necessarily identical. And it should be mentioned that in superconductors there is also a relaxation time with respect to diffusion of magnetic flux density the comparison of which with thermal relaxation time in superconductor and matrix material has lead to development of multi-filament composite wires.

The situation can be compared with current injection experiments (see for example [13, 14]): There, the decay of electronic excitations is studied after an artificial increase of the number of quasi-particles. Here,

we have an increase of this number from decay of electron pairs if sample temperature, T, increases (but $T < T_{Crit}$), with the total number of particles conserved. Also, current injection experiments deal with thin films, here we investigate solid samples (YBCO pellets).

During levitation experiments, traditionally a decision between "levitation or not" is based entirely upon observation of *bulk temperature*, T(t), below critical temperature, T_{Crit}. We instead in [6] made this decision on the basis of the *internal* temperature excursions, T(x,y,z,t) which generate a non-zero levitation force from each of the N volume elements only if the corresponding element temperature is below T_{Crit} and the vector sum of all contributions to levitation finally overcomes the sample weight. The question then is whether during cool-down the re-arrangement of the corresponding wave function (anti-symmetric for electron pairs), as a response of the electron system of the superconductor to the thermal disturbance, really keeps step with the temperature excursion of the lattice (the phonon aspect) to re-establish dynamic equilibrium between generation of electron pairs and their decay to quasi-particles.

For a provisional comparison of τ_{Ph} and τ_{El}, consider a thin YBCO film of d = 0.1 μm thickness onto which a very short thermal pulse (a "Dirac pulse" from a laser) is delivered. The small thickness, d, is assumed just to compare with thin superconducting metallic films in current injection experiments. Assuming the thermal diffusivity, a, of the YBCO film is constant (independent of temperature) and considering only the dominating (n = 1) term in a series expansion of T(t) (see *e.g.,* [15]), the time constant $\tau_{Ph} = d^2/(a\,\pi^2)$ of the film amounts to about 0.3 ns at T = 90 K. This is definitely smaller than τ_{El}, the lifetime of disturbed states which is on the order of 0.1 to tens of μs [13, 14] observed in current injection experiments using Al or Sn films of same thickness.

Measurement of quasi-particle recombination time (lifetime of the disturbed electron system) in superconducting tin after current injection from a current pulse or from laser pulse excitation was performed in [14] with current $i_P = 10.1$ mA and $t_p = 1$ μs the length of the current pulse. There are about 6.3×10^{10} unit charges injected into a volume of at least 3×10^{-14} m^3, which means an injected particle density of about 2.1×10^{24} $1/m^3$ (see [14], Fig. **3**). On the other hand, after a thermal disturbance in YBCO, we have a probability for exciting quasi-particles from pairs proportional to $\exp[-\Delta E(T)/kT]$. Here we use the equilibrium expression. Assuming that a HTSC sample was heated locally from 90.5 to 91.999 K and using the electron density at temperature close to absolute zero of about 6×10^{27} $1/m^3$ of which about (½) (1/10) is available for pair formation, the volume in which current was injected in [14] and a standard (BSC) temperature dependence of $\Delta E(T)$ [16], this yields the number of additionally excited electron states in the same volume of about 4.7×10^{26} $1/m^3$, or about two orders of magnitude larger than in the current injection experiment, as a lower limit.

Therefore, a naive estimate of the lifetime $\tau_{El} = \tau_{El,therm\ excit}$ could be made by $\tau_{El,therm\ excit} = M\ \tau_{El,Current\ inject}$, with $\tau_{El,Current\ inject}$ on the order of 0.1 to 1 μs and $M \geq 10^2$. This would result in a τ_{El} of at least 10 to 100 μs for the thermal disturbance, much larger than τ_{Ph}, if the temperature is not too close to T_{Crit}. Note that the current injection experiments were performed in [14] at temperature below 2 K, safely below T_{Crit} of Sn of 3.72 K and that the quasi-particle diffusion length in the present experiments is much smaller than the sample thickness which means there will only be little escape of phonons.

To improve understanding of experiments focussed on possible weight anomalies in superconductors during phase transition, the generation rate of electron pairs as bound states in superconductors and their decay to quasi-particles as a dynamic equilibrium process or under thermal excitation and recombination thereof, have to be analysed. Like a variety of other excitations in superconductors (absorption of micro-waves, steady-state or pulsed tunnel diode experiments, absorption of incident phonons by the lattice), decay of thermal excitations of the electronic system can be described as relaxation of strongly populated non-equilibrium states.

Dynamic (experimental) equilibrium generation or decay rates, $G_{exp}(t)$, of electron pairs (EP) initiated by propagation of a thermal disturbance resulting entirely from phonon interactions were estimated from

$dN_{SC}(t)/dt$ using $N_{SC}(t)$ from Fig. **14** and the equilibrium density, ρ_{EP}, of this material for the 4 experimental conditions (items 1-4). Results are shown in Fig. **15**.

Note that the rates shown in Fig. **15** are given per unit of sample volume. If taking instead the differentials dV_{SC} of the volume elements that have become superconducting or normal conducting, respectively, the rates of items (1) to (4) of course would be identical. But it takes the superconductor a finite time, Δt, to induce screening super-currents over the *whole* sample surface (which again reflects the time interval to re-arrange the wave function of the whole electron system) so that the lifetime of the excited states in the sample (4) must be short enough to satisfy the rates $G_{exp}(t)$.

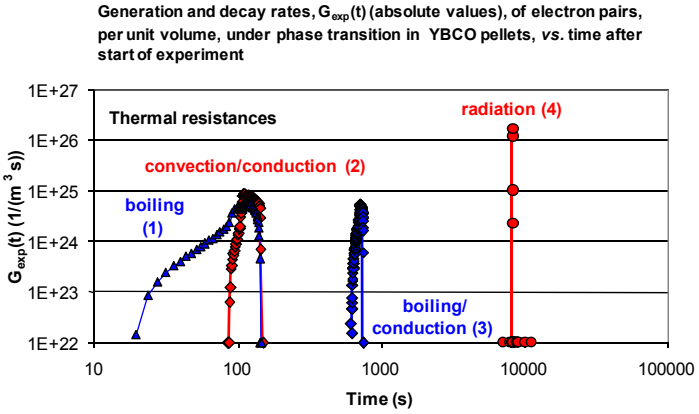

Figure 15: Generation and decay rates, per unit sample volume, *vs.* time after start of the experiment, with the location of the phase transition on the time axis resulting from the thermal resistances, items (1) to (4), and the corresponding temperature intervals, ΔT between T_{Crit} of the sample and corresponding environment (see text). The rates $G_{exp}(t)$ are calculated from the product $\rho_{EP}\ dN_{SC}(t)/dt$ using the $N_{SC}(t)$ from Fig. **14**. Only rates exceeding 10^{22} 1/(m^3 s) are plotted in this figure.

Up to this point, we have considered only temperature excursion, T(x,y,z,t), *i.e.,* the *phonon* aspect of propagation of a thermal disturbance and its consequences. That is, $N_{SC}(t)$, its derivative $dN_{SC}(t)/dt$, and the equilibrium density of pairs - a temperature dependent quantity. Calculation of the theoretical decay rates, $G_{NE}(t)$, the response of the *electron* system to the disturbance, and the decay of the *result* of this disturbance (eg during warm-up: decay of electron pairs to an increased number of quasi-particles) now follows.

3.2. Non-Equilibrium Decay Rates

Non-equilibrium rates, $G_{NE}(t)$, are modelled as sequential generation or decay events with lifetimes estimated either from the uncertainty principle or by analogy to an aspect of the nucleon-nucleon, pion-mediated Yukawa interaction. In a later publication we will report on a diffusion model approach where we imagine that the concentration of bound electron states finally arrives at equilibrium when it "diffuses" through the sample volume. This is also related to diffusion of magnetic flux density in superconductors. The number of excitations, N_{Exc}, is proportional to $\exp[-\Delta E/kT]$, with ΔE the width of the energy gap. Though an equilibrium quantity, it can be taken as an approximate measure of the "disturbance" of the wave function that has to be re-established to its dynamical equilibrium shape. Lifetime of an excitation then is understood as the (relaxation) time, τ_{El}, that the disturbed anti-symmetric wave function, determined by N_{Exc} among other dependencies, will require to be re-arranged to properly describe the return to dynamical equilibrium while respecting the Pauli exclusion principle. Lifetime, τ_{El}, thus determines average rates, $G_{NE}(t) \sim N_{Exc}/\tau_{El}$, to which the experimental $G_{exp}(t)$ finally are compared.

Comparing the experimentally-confirmed simulations to the theoretical modelling (Fig. **16**), a discrepancy appears between both rates, $G_{exp}(t)$ and $G_{NE}(t)$, if temperature is very close to critical temperature (left section of

Fig. **16**) and, in particular if the pellet is warmed-up solely by radiation, the highest thermal resistance situation, which means a small Biot number, taking account the thermal conductivity of the YBCO pellet material.

The theoretical rates, $G_{NE}(t)$ indicated by diamonds, were obtained for constant temperature meaning also the rates are constant. For comparison, maximum values of the experimental $G_{exp}(t)$ are also plotted (taken from Fig. **15**), indicated by blue and red horizontal dashed lines which refer to boiling/convection/conduction and radiative resistance (items 1 and 4, the extreme cases among the above), respectively. Open and closed diamonds indicate initial and average decay rates of excitations, respectively, the average taken over a volume V_C the size of which is given by a screened Coulomb potential between electrons that couple to **S** = 0, **L** = 2 pairs, as is typical for unconventional superconductors. Generally, the problem is that because of numerical reasons a very small volume has to be taken for calculating averages of $G_{NE}(t)$, but it must be large enough to reasonably compare with the $G_{exp}(t)$. Provisionally, screening factors between 1 and 0.01 of the Coulomb potential for two single unit electron charges have been assumed in the calculations but even the 0.01 value may still be too large in comparison with a Thomas-Fermi potential. Here the problem is to identify a reasonable value of the Thomas-Fermi scattering length of HTSC from the literature.

If the energy gap, ΔE, was constant and independent of temperature, the logarithmic dependence of the decay rates shown in Fig. **16** would be linear in $\Delta E/kT$, as is the case in a typical Arrhenius plot. But ΔE depends on temperature so that a linear relationship between the decay rates and $\Delta E/kT$ is observed only in a log-log plot.

Apart from considerable uncertainty of the screening factor, Fig. **16** suggests the theoretical rates (full and open diamonds) decrease strongly when temperature ($T < T_{Crit}$) approaches T_{Crit} during warm-up periods (left section of Fig. **16**, see figure caption).

The results given in Fig. **16** are obtained at *constant* temperature. If temperature differs from T_{Crit} by *e.g.,* only 10^{-6} K, and if T is constant, the "driving force" (the differences in free enthalpy of the system) approaches zero, which means in the limit $T = T_{Crit}$ the system finally has returned to dynamic equilibrium, now at the phase transition, as a state with only statistical fluctuations of the populations of pairs and quasi-particles. Intuitively, one would say the system then is frozen: the more the temperature approaches T_{Crit}, the smaller the variation of both populations and the longer the lifetime of the (residual) disturbed state, as is predicted by Fig. **16**. However, T = T(t) during cool-down or warm-up periods and the theoretical rates (G_{NE}, constant in Fig. **16**) will change with time. The interplay of two time constants, in the present case τ_{Ph} and τ_{El}, has to be taken as a function of time.

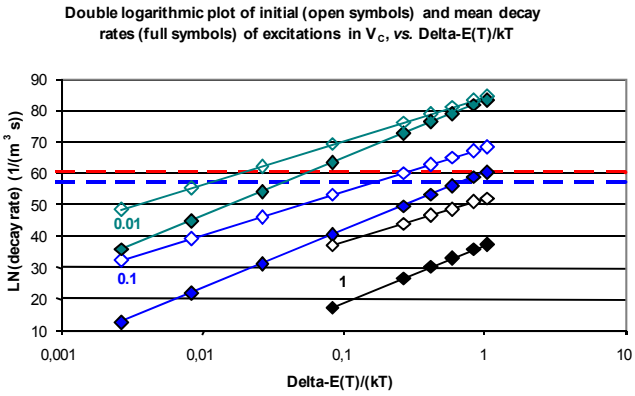

Figure 16: Comparison of experimental, $G_{exp}(t)$ (dashed lines on the ordinate), and theoretical decay rates, $G_{NE}(t)$ (diamonds), assuming different screening factors of the screened Coulomb potential between two electrons in a solid, with ΔE the energy gap of YBCO. Data are given for *constant* temperature, which means the calculated rates are constant at the corresponding temperature. Open and solid symbols indicate initial (immediately after the start of the disturbance) and mean (average taken over the whole time interval needed for return to equilibrium) decay rates, respectively. The curves are given between abscissa values from very close to $\Delta E(T)/kT_{Crit}$ (left section) to $\Delta E(T)/kT$ with T = 91.5 K (right section of the figure).

As a consequence of the difference between τ_{Ph} and τ_{El}, or the difference between both experimental and theoretical rates, we observe a "dead time" interval on the T(t)-scale, which may dissolve or smear out signals that otherwise would be clearly observable (levitation, break-down of super-currents, or the jump of the specific heat at the phase transition, to mention only a few). The same conclusion applies if it is expected that a correlation (if any) of gravity with superconductivity could be detected at the phase transition. In particular, if smear-out occurred just during the interval when temperature was measured in the suspension balance experiment [5], the signal (if any) simply would be lost. For an initial estimate of the dead time interval, we could take the lifetime estimated above from current injection experiments, but this needs more investigation using the above mentioned models to properly indicate its value.

The same situation arises if in any experiment the external heat transfer to the sample is weak in comparison to a much stronger internal heat conduction. In Fig. **15**, this case is reflected by the tiny half-width of the decay rate obtained under boundary conditions of item (4). Note that the peak value of this curve dominates in Fig. **15**. Pure radiation heat transfer means a small Biot number so that in a warm-up experiment, all volume elements *simultaneously* become normal conducting as soon as the temperature field, T(x,y,z,t), for all x,y,z within the sample volume, reaches T_{Crit}. This in turn indicates the theoretical decay rate per unit volume must be enormous to keep pace with the phonon excitations.

Initial simulation results (Fig. **16**) indicate that it is uncertain if the theoretical decay rates will be large enough very near to the phase transition. There is no doubt that all volume elements of the pellet used in, for instance, the suspension balance [5] finally arrived at normal conduction. But the real question is; after what length of time after start of warm-up did the electronic states during the experiment arrive at dynamic equilibrium? Or, reversing the question; is it really desirable to look for intermittently occurring *sharp* signals in this or similar experiments to detect correlations of gravity with phase transition? Or would it be more reasonable to look for differences between initial and final sample weight in gravity experiments (group 1 of the above)? More investigations are underway to address these questions, and details and results will be reported in another contribution to this volume (H. Reiss, Impact of Lifetime and Decay Rates of Thermally Excited States in Superconductors on a Gravity Experiment).

4. CORRELATION OF MASS ANOMALIES WITH INTRINSIC PROPERTIES OF SUPERCONDUCTORS

If superconductivity can be considered as a pathway to *mass* anomalies, a rigorous correlation, not just coincidence, between two *intrinsic* materials propertie*s* has to be demonstrated: a negative free enthalpy difference between normal and superconducting states, and a change of rest mass. If on the other hand a weight anomaly should have its origin in a gravity field anomaly, correlation between an *intrinsic* materials (*e.g.,* HTSC) property with an *extrinsic* variable (the gravity field) has to be verified.

The free enthalpy difference of type I or type II superconductor materials is maximum between the normal conducting and Meissner states. If mass anomalies resulting from being in the superconducting state really existed, they would be destroyed if the material leaves the Meissner state. If the existence of the Meissner state cannot be demonstrated in, for example, binary, ternary or quaternary diborides or borocarbides or other new classes of HTSC such as recently-reported zero-resistance in nano-sized Au-wires [17], none of them is a superconductor. By analogy, if it cannot be demonstrated that mass anomalies are rigorously coupled to the existence of the Meissner state, the observed anomalies cannot have their origin in superconductivity. Existence of a correlation between the two intrinsic variables has been investigated when samples were exposed to a magnetic field strong enough to destroy the Meissner state ([1] is apparently the only experiment that specifically was designed to determine such correlations).

5. GRAVITY ANOMALIES

In Podkletnov's experiment [3] the weight anomaly in a test sample, eg SiO_2 can be attributed only to a variation of an *extrinsic* variable (the gravity field). The SiO_2 test mass temperature or other intrinsic thermodynamic properties should not have had any (direct) impact on the experimental result. It was not

clear in this experiment whether the total external field on the rotating superconductor resulting from both the levitation solenoid and the multi-phase RF coils was smaller or larger than the lower critical field of the rotating HTSC disk material itself. Both the Meissner effect and Shubnikov phases of superconductors allow levitation, with different levitation heights, however. The resulting field at the disk's surface might well have been above the lower critical magnetic field and the disk then would have experienced hysteresis losses during rotation which would likely have increased the disk's temperature. However temperature measurements were not reported and the only indication the disk was in a superconducting state was its apparent levitation above the levitation solenoid.

Proof of a gravity field anomaly in the Podkletnov experiment thus must concentrate solely on the elimination of possible existing disturbances of the weight measurement such as convection or buoyancy superimposed on gravity. In his published report, Podkletnov used a thin foil to shield the test mass from direct contact with up-streaming evaporated helium gas and gas convection arising from gas/solid friction at the surface of the rotating disk. But the foil is cooled by the up-streaming He vapour to temperatures well below room temperature. Condensation of water vapour and a corresponding down-streaming of air from the atmosphere onto the upper foil surface then is superimposed onto gravity, leading to complicated flow patterns in the vicinity of the freely hanging SiO_2 sample. Considerable convective effects would prevail even if the sample is shielded in a protective tube but filled with atmospheric air. As in Hathaway [4] a good thermal insulator should have been used as a shield instead of a simple thin, thermally transparent foil.

In order to reveal a possible correlation in the Podkletnov experiment, the origin of the claimed gravity anomaly has to be identified. Simple replacement of the HTSC disks by normal- or non-conductors would not modify the gravity field to any measurable extent. This replacement *a priori* would not be able to either confirm or reject a suspected correlation. By analogy, a correlation between the operation of two thermodynamic "machines" A and B in which A assumes two different states (like A_1: Meissner, A_2: non-conducting) cannot be confirmed or rejected if one of the two machines (A) is replaced by a third, C, that can assume only one state, in this case a non-conducting disk. The claims reported in Podkletnov [3] would thus reduce to simply a coincidence between levitation and rotation of a HTSC disk and a suspected gravity anomaly.

6. EXPERIMENTAL ISSUES IN THE SEARCH FOR MASS OR GRAVITY ANOMALIES: TRAPS AND PITFALLS

Experiments designed to search for mass anomalies generally involve the use of high–sensitivity balances operating either in atmosphere, or preferably, in vacuum. Such balances should ideally be isolated from disturbances arising from seismic influences in the vicinity and may even necessitate taking account of tidal or diurnal effects depending on their sensitivity. Electronic balances incorporating electrically-driven strain-detection elements must be shielded from electromagnetic fields arising from sources in the vicinity, either from the experiment itself or the power and control electronics nearby. This, of course, also applies to balances used in the search for gravity field anomalies. As the use of HTSC materials necessitates extremes of temperature in the neighbourhood of the balance, special care has to be taken in balances based on a moving arm or torsion element to ensure that the various structures are not affected either by thermally-induced length changes or by even minuscule amounts of vapour condensation.

The search for gravity field anomalies involves experiments designed to look for anomalous forces on the matter making up test masses. The experimenter must be aware that there are conventional explanations for most of the apparent anomalous forces seen in such experiments. Since most balances used for such experiments are operating at the limit of their sensitivity, many subtle influences come into play which are not always immediately obvious. In general, the two most powerful external effects are magnetostatic and electrostatic. As superconductors are forced above and below their transition temperature, trapped fields can be suddenly released, affecting magnetic materials in the vicinity. This is true for static magnetic fields operating on magnetic balance or container materials and for quasi-static fields inducing Lenz effects on conductors. The use of high voltages, *e.g.,* for powering levitation coils, can induce surface charges on non-conducting test masses which have been insulated both electrically and thermally from their surroundings.

If nearby support structures and containers are not completely free of polar molecules such as water films, there can be electrostatic forces between the films and test masses which may result in unusual balance readings which coincide with some activation of a portion of the experiment. Charged elements such as test masses or balance components can be attracted to or repelled from electric field gradients as in electrophoresis. Typically, however, forces proportional to v x B are usually negligible.

Samples which are non-uniform in density or composition result in spatial gradients of thermal properties which can be affected by subtle but conventional thermal influences. Thus precise descriptions of materials preparation and composition have to be reported to distinguish a possibly existing gravity anomaly from prosaic explanations and artefacts. This of course applies to all experiments of group 1 or 2.

In the course of trying to measure signals from potentially minuscule (if existent) forces, constant vigilance for more prosaic explanations must be maintained. This is true when measuring not only the type of force (*e.g.,* magnetic, electrostatic, mechanical, gravitational), but also the origin of the force. In even the most carefully designed experiments, it is easy to be fooled by a litany of potential effects resulting from experimental procedures that may have been poorly conceived or carried out. This section provides a brief overview of some of those considerations.

For example, the direct determination of the mass of a test sample cooled to cryogenic temperatures typically requires that the test sample be attached to a measurement device (a balance for example). If the balance is not cooled, the connection between test sample and instrument must accommodate a very great temperature difference, and problems may arise due to condensation and buoyancy as discussed above. In order to shield the test sample from the effects of condensation, the sample can be enveloped either in a vacuum or a non-condensable (at the operating temperature) gas. Placing the sample in a vacuum mitigates both buoyancy and condensation concerns, but may preclude effective cooling of the sample and its precise temperature measurement. Hence a compromise must be struck between the need to isolate the sample from the environment and the speed at which cooling is expected. Balances which operate in vacuum are useful in this regard.

Determination of the weight of a test sample which is near a superconductor, such as that in Podkletnov's experiment [3], requires that the test sample be isolated from the environment as much as possible, to avoid being shaken, buoyed by air or gas currents, or otherwise perturbed. However, since the sample itself may not need to be cooled, the requirement for strict temperature isolation can be somewhat relaxed.

Exacerbating the problems inherent in cryogenic experiments are those introduced by nearby electric and magnetic fields. As the experimenter endeavors to increase the mechanical isolation between the test sample and the local laboratory environment, the sample's susceptibility to electromagnetic and electrostatic influences becomes greater.

The following summary of the some of the more important experimental concerns is organized into general categories, and there will inevitably be some overlap. It is by no means exhaustive.

6.1. Mechanical Effects

6.1.1. Thermal Effects

This includes thermally-driven air, gas or liquid currents, vapor condensation, and thermal expansion issues when a difference in temperature is encountered. Thermally driven currents act to artificially alter the weight of test samples they encounter. It is often exceedingly difficult to calculate the resulting forces, which tend to randomly fluctuate both temporally and spatially. Condensates can alter the mass of the test article, with the most problematic condensate in cryogenic experiments being water vapor from the air, and, to a lesser extent, oxygen and nitrogen condensate when working at LHe temperatures. Experiments must be designed to avoid any part of a cryogenically-cooled apparatus being in contact with condensable gasses. When dealing with severe temperature differences, structural apparatus and other test articles must not be subjected to thermal expansion or contraction, unless this effect can be accurately analyzed and factored into the resulting measurements.

6.1.2. Buoyancy Effects

Materials display different buoyancy in different media. If a test sample is weighed in air, then weighed in LN_2, its apparent weight will clearly differ and be shape-dependent. More subtly, if the sample is cooled to cryogenic temperatures, its buoyancy cross-section changes as a function of its temperature, producing a time-varying weight change that could be misinterpreted as a gravitational interaction. Buoyancy differences may also arise in a single medium (such as air) due to stratification and temperature differences in the medium.

6.1.3. Seismic/Vibration Effects

Scales, balances and force sensors generally operate by detecting or displaying the relative distances between fixed and movable masses, and it is necessary to avoid introducing artificial mechanical motion/noise into the measuring system. Vibrations can occur from laboratory and other sources, such as compressors, fans, and local traffic (both pedestrian and vehicular), and are usually transmitted into the measuring apparatus by structural elements. Mitigation is typically achieved either by loosening the structural design through the installation of dampers, or tightening the design by anchoring the support structures to larger, relatively immobile masses. If these are not easily or completely achievable, altering the frequency of the chief modes of vibration by adding or subtracting masses is often helpful. Wires and cables carrying signals and power may appear negligible as structural vibration carriers, but for experiments at cryogenic temperatures the wires may freeze and become rigid. In addition, the pulsing of current through any portion of a wire with curvature will produce a flexure in the wire, leading to displacement or, for alternating currents, oscillatory vibrations. The possibility also exists that the measuring system is non-linear over some or all of its range and may suffer from hysteresis or viscous effects which can lead to apparently steady but erroneous readings due to partial rectification of external vibrations. For example it is well-established that vibration applied to a standard analytical chemical balance will cause its steady readings to drift because the air dashpot or similar damping device is non-symmetrical and can apply more force in one direction than the other.

6.1.4. Vacuum Effects

All materials will to more or less extent outgas (release vapor) in vacuum, hence the use of low-outgassing materials for any experiment performed in a vacuum or low ambient pressure environment is desirable. Even a low outgassing material may have minute amounts of contaminant (oils, fingerprints, *etc.*) on its surface, the release of which can be detected by sensitive balances. Other contaminant material on the inside walls of the vacuum chamber housing the sample may be released and coat or otherwise impinge upon the sample. Of more subtle nature is the slight movement of the vacuum chamber and encompassed test apparatus as the vacuum chamber is pumped down. Such small movements can offset previously aligned balances, producing an apparent weight change in a test sample simply due to a slight shifting in the support structures. It is also worth noting the high degree of variation in outgassing between materials which may be used in test apparatus or support structures involved in such experiments. For instance, brass has a high outgassing rate due to the presence of high vapor pressure zinc; if a brass test mass is used in a vacuum environment, it's actual weight loss could change over the course of the experiment and mask other experimentally-induced effects.

6.1.5. Liquid Effects

The evaporation or boiling of liquid (usually the cryogen) around a test sample or the suspension system can clearly contribute noise into the measurement system. This is particularly true when the test sample is suspended in, or is in contact with, a liquid cryogen used to cool it below its transition temperature. Boiling of the cryogen when inserting a sample will cause spurious readings and potentially mask effects near the critical temperature until sample and cryogen are in thermal equilibrium. Similarly, lifting the sample from a cryogen produces high rates of evaporation (often in addition to dripping cryogenic fluid), and will cause an apparent weight change as the temperature of the test sample rises back to ambient thermal conditions.

6.2. Temporal Effects

Certain experiments require a test sample to be cooled in cryogenic gas or liquid while being suspended from the movable arm of a balance. The precise determination of sample temperature as a function of time

is critical to ascribing an observed weight change to a superconductive attribute. However, the attachment of a thermocouple to the superconducting sample necessitates feeding wire leads from the movable sample to the fixed laboratory frame on which the temperature readout sits. Movable slip rings are too stiff and unpredictable to be used as rotating/movable joints in most delicate experiments. Testing for the attainment of critical transition temperature *via* Meissner flux expulsion is often too cumbersome, and would of necessity disturb the balance. If direct temperature determination proves exceedingly difficult, the best path is for the experimenter to simply allow sufficient time for the test sample and any supporting mass to reach the required equilibrium temperature.

Additionally, if the expected gravity effects are correlated with a narrow transition around T_{crit}, the caveats in Section 3 should be noted.

6.3. Electromagnetic Effects

6.3.1. Magnetic Coupling

The incorporation of superconductors in gravity experiments necessarily involves magnetic fields. Potential interactions with the magnetic fields arising from current-carrying and signal wires must be taken into account in the vicinity of the experimental apparatus. Residual magnetism can be found in certain "non-magnetic" metals and alloys, which may interact with the measurement system. The assumption of perfect magnetic shielding by high-mu magnetic shielding alloys is usually not valid, and care must be taken that the proper level of electromagnetic shielding required by the experiment is obtained. Time-varying electromagnetic fields generated by test equipment, power sources, leads, and contacts can interact with nearby conducting bodies and cause often subtle but nevertheless spurious measurements. More dramatically, the sudden release of trapped magnetic fields in superconductors raised above transition temperature can affect, and be affected by, nearby magnetic or conductive structures.

6.3.2. Electric Coupling

As in the use of high-mu metals to shield magnetic fields, an over-reliance on a Faraday Cage for complete exclusion of DC or quasi-static electric fields is often not realistic, and extreme care should be taken to account for and mitigate any spurious electric fields that may interfere with the test specimen or measurement apparatus.

6.3.3. Electromagnetic Coupling

Improper shielding or conductor pairs that are not tightly twisted can cause unwanted crosstalk on nearby signal cables, even shielded ones. Switching transients in high-power circuits can easily couple into signal sensing circuits, causing artificial or spurious readings; this is particularly important for circuits incorporated into electronic balances. Using RF power with improperly-matched loads or inappropriately sized matching networks can cause intense electromagnetic interference in nearby circuits.

6.3.4. Grounding Issues

The physical layout of signal grounds should be carefully considered to avoid nearby magnetic interference. Shield grounds should be checked for potential ground loop problems by incorporating a single-point grounding connection. Contacts should be checked for loose, corroded, or bi-metal connections which can introduce unwanted contact potentials.

6.4. Electrostatic and Related Effects

6.4.1. Gradient Effects

The operation of an apparatus at high DC voltages relative to a nearby ground will usually produce spatial gradients in the electric field, unless the experiment is specifically designed to produce uniform fields in the vicinity of the test apparatus. Such gradients may induce subtle motion in nearby free bodies whether conductive or not, such as samples suspended from a balance.

6.4.2. Charge Pooling and Induced Charges

Even under high vacuum, without sufficient surface preparation and thermal baking, the interior surfaces of vacuum chambers are covered with invisible pools of surface charges, usually in the form of films of polar water molecules. In very sensitive measurement systems, or where the sample mass being weighed is in close proximity to a wall, the electrostatic forces between such "patch charges" on the wall and test mass may interfere with proper weight measurements. This applies whether or not the surfaces are conductive.

6.4.3. Ion and Molecular Effects

In high-voltage DC or AC experiments, even in vacuum, strong electric fields can accelerate outgassed or residual ions in the vacuum chamber, which in turn can impart momentum to a suspended test mass. This may occur either because the ions are streaming off of or on to a sample held at high voltage, or because the sample may be in the "ion wind" produced by a nearby source of ions held at high voltage. Such ion wind effects are difficult to calculate, and so generally need to be avoided by adhering to strict chamber cleanliness procedures, proper choice of vacuum compatible materials (including wire insulation), and operation at chamber pressures below those needed to produce significant ion wind effects. High voltages can cause ablation or sputtering of even the best insulation.

6.4.4. Charge Leakage

Charges can leak from insulated conductors, either as a quasi-DC corona or (more likely) in bursts called Trichel Pulses in high-voltage experiments. These may be negligible to the force-measuring apparatus at relatively low voltages, but at some threshold value they can suddenly become problematic, and often under generally unpredictable conditions. These can cause direct effects, for instance by impinging on or interfering with balances, or indirect effects through, for example, interference with nearby signal wires. Most commonly, they cause weak conduction paths to nearby grounds which can interfere with high-gain amplifiers, *etc.*

6.5. Experimental Expectations

The above list is but a small sampling of the experimental artifacts that must be considered when designing and performing any sensitive laboratory experiment, and particularly when searching for minuscule effects in support of controversial theories. In addition, there are psychological pitfalls that investigators designing experiments are often not aware of. For instance, *confirmation bias* is the tendency to trust data that supports one's hypothesis, and to distrust (or ignore) data that does not support it. After all, if my data is exactly as my theory predicts, then the experiment is a good one and I made no errors! Another is *errors in logic*. An example of one such incorrect syllogism might be "If A is true, then we will observe B. We do observe B, therefore we have proven A is true". This false logic overlooks other explanations for observing B. Put more correctly the logical statement is: "We do observe B, therefore one possible explanation is that A is true, and there may be other explanations." The all too common *neglect of prior probability* flouts Bayes' theorem, which shows that if the probability of a theory being true before the experiment is low, then a stronger standard of proof is required to support its correctness. These and other considerations must be recognized and added to the usual repertoire of experimental design and protocol which makes up the bulk of the scientific method.

7. APPLICATION OF DATA ANALYSIS

Anomalies and correlations between intrinsic and extrinsic variables can be demonstrated using standard statistical methods like Gaussian fits to scattered data, calculation of correlation coefficients, χ^2-analysis or confidence intervals. Only a very few papers presented on gravity anomalies include error estimates that are necessary to clearly separate an anomaly from an artefact. Application of χ^2-analysis to an appropriate hypothesis without error bars is useless. Error analysis including, *e.g.,* full balance specifications, requires understanding the chain by which individual experimental errors propagate and this implies at least an attempt at a physical model to explain the putative gravity anomaly. Errors introduced by subtle influences such as outlined in the previous sections have to be incorporated. At the very least, these have to be reasonably estimated, if not provided by separate calibration or manufacturer's specification. The same applies to temperature control. Although superconductivity is essentially a cryogenic temperature

phenomenon, little attention is paid in many papers to noise levels resulting from the attainment of thermal equilibrium, how to appropriately measure temperature gradient fields, the estimation of parasitic heat flow and the impacts of radiation fields.

In order to safely separate anomalies from prosaic phenomena, a sharp criterion like a 6σ-distance between the corresponding mean values seems appropriate. Overlap of standard deviations, σ (the "noise"), then will be excluded with very high statistical significance.

8. CONCLUSIONS

Experiments to detect mass or gravity field anomalies using weight measurements of HTSC samples should ideally employ magnetic suspension balances that house the samples in a vacuum and use strict temperature monitoring and control, such as used by Tajmar [5]. All experiments including suspension balance measurements have to be designed in such a way as to exclude conflicts between different relaxation rates of thermal transport mechanism during cool-down or warm-up periods, and the response of the electronic system of the superconductor material to the same disturbances. Detection of such anomalies using a non-HTSC test mass in the vicinity of an HTSC should ensure that the test mass is suitably isolated from the ambient environment. Provisions have to be made to switch the superconductor between superconducting and non-superconducting states by applied magnetic fields. Knowledge of the likely prosaic explanations for the observations, and thorough error analysis are indispensable.

REFERENCES

[1] Reiss H. Weight Anomalies Observed During Cool-down of High Temperature Superconductors. Phys Essays 2003; 16: 236-253.

[2] Tajmar M, Hense K, Marhold K, de Matos C. Weight Measurements of High Temperature Superconductors During Phase Transition in Stationary, Non-stationary Conditions and under ELF Radiation. In: M.S. El-Genk, Ed. Space Technology and Applications International Forum (STAIF-05). American Institute of Physics 2005.

[3] Podkletnov E, Nieminen R. A Possibility of Gravitational Force Shielding by Bulk $YBa_2Cu_3O_{7-x}$ Superconductor. Physica C 1992; 203: 441-444.

[4] Hathaway G, Cleveland B, Bao Y. Gravity Modification Experiment Using a Rotating Superconductor Disk and Radio Frequency Fields. Physica C 2003; 385: 488-500.

[5] Tajmar M, Plesescu F, Seifert B. Measuring the Dependence of Weight on Temperature in the Low-Temperature Regime Using a Magnetic Suspension Balance. Meas Sci Tech 2010; 21: 015111.

[6] Reiss H, Troitsky O Yu. The Meissner-Ochsenfeld effect as a possible tool to control anisotropy of thermal conductivity and pinning strength of type II superconductors. Cryogenics 2009; 49: 433-448.

[7] Reiss H. A numerical analysis of shield temperatures, heat losses and residual gas pressures in an evacuated super-insulation using thermal and fluid networks, Part I: Stationary Conditions. Cryogenics 2004; 44; 259-271.

[8] Sandner S. Stoffwerte von reinen Metallen und Metall-Legierungen. In: VDI Heat Atlas, 10th Ed. Springer 2006; Chapters Dea1 - Dea2.

[9] Touloukian Y, DeWitt D. Thermal radiative properties-Metallic elements and alloys. In: Thermophys. Properties of matter, Vol. 7. IFI/Plenum 1970; p. 137.

[10] Kabelac S, Vortmeyer D. Strahlung technischer Oberflächen. In: VDI Heat Atlas, 10th Ed. Springer 2006; Chapters Ka1-Ka11.

[11] Kaganer M. Thermal insulation in cryogenic engineering. Israel Progr Sci Transl 1969; 33-34.

[12] Klan H. VDI Heat Atlas, 10th Ed. Springer 2006; Chapters Fe1 - Fe3.

[13] Gray K. Steady State Measurements of the Quasiparticle Lifetime in Superconducting Aluminum. J Phys F Metal Phys 1971; 1: 290-308.

[14] Epperlein P, Lassmann K, Eisenmenger W. Quasiparticle recombination time in superconducting tin and normal electronic density of states at the Fermi surface from tunnel junction experiments. Z Physik B 1978; 31: 377-384.

[15] Carslaw H, Jaeger J. Conduction of Heat in Solids. Oxford Science 1959; p. 94.

[16] Blatt J M. Theory of Superconductivity. Academic Press 1964; p. 243.

[17] Takayanagi K. Preparations of Gold Nano Wire with Helical Multi-Shell. MEXT press release. Tokyo Inst Tech, July 21, 2000.